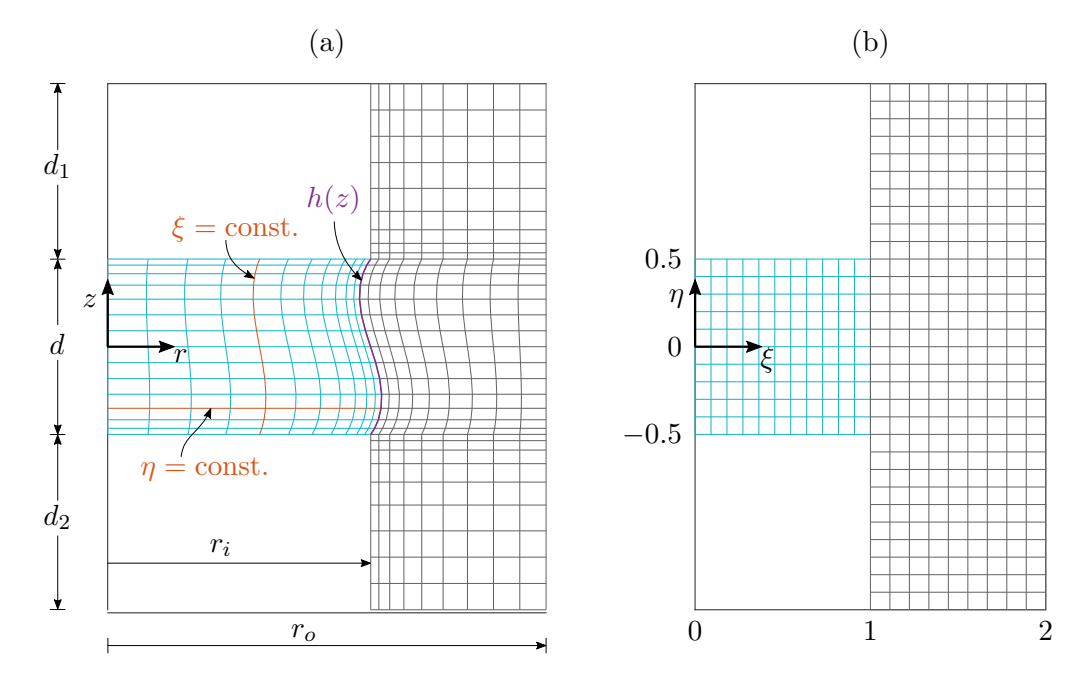
## **Discretization**

MaranStable has been designed to compute the stability with respect to small perturbations of a steady two-dimensional flow flows in canonical geometries that are either axisymmetric or infinitely extended in the third dimension. Independent of the geometry selected, MaranStable first computes the basic flow, varying in the first and second spatial dimension, that is defined by the fluid model and the boundary conditions. Thereafter, the evolution of perturbations to the basic flow are considered in form of Fourier modes which are periodic in the third (homogeneous) dimension. Assuming the perturbations are small they decay/grow exponential in time. The evolution equations for the Fourier modes leads to eigenvalue/eigenvector problems that provide the growth rates, frequencies and the normalized structure of the Fourier modes in the first and second dimension. MaranStable returns the most-dangerous Fourier mode which has the largest growth rate.

Both, the basic state equations and the linear stability equations are discretized on the same mesh using the same discretization method. The two-dimensional mesh is independent of the coordinate system employed (Cartesian or cylindrical). As an illustrative example, we focus on cylindrical coordinates (r,z) with the understanding that the discretization is formally identical for Cartesian coordinates (x,y).

As can be seen in figure 1(a), MaranStable employs coordinates that are body-fitted to the interface h(z) between liquid (blue) and gas (black). Instead of discretizing the governing equations on the physical mesh, MaranStable first maps the deformed mesh onto a computational mesh (see figure 1(b)) with new coordinates  $(\xi, \eta)$  by means of the



**Figure 1:** Illustrative examples for the different types of meshes. (a) Physical mesh with characteristic lengths and radii. (b) Transformed computational mesh.

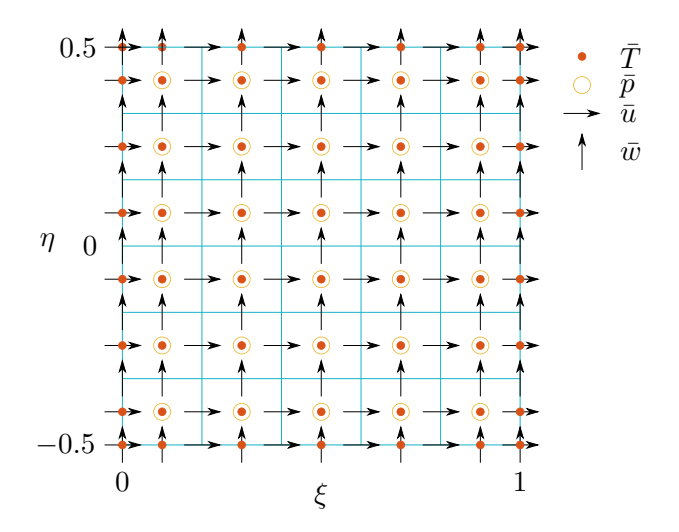


**Figure 2:** Collocation of the field quantities on the staggered computational grid.  $\bar{T}$ : Temperature.  $\bar{p}$ : Pressure.  $\bar{u}$ : Radial velocity component.  $\bar{w}$ : Axial velocity component.

coordinate transformation

$$\xi(r,z) = \begin{cases} \frac{r}{h(z)} f_{l}(r) & \text{for the liquid phase,} \\ \left[1 + \frac{r - h(z)}{r_{o} - h(z)}\right] f_{g}(r) & \text{for the gas phase,} \end{cases}$$
(1a)

$$\eta(z) = \frac{z}{d}g(z),\tag{1b}$$

where  $f_1(r)$ ,  $f_g(r)$  and g(z) are inverse stretching functions that are applied to rearrange the cells equidistantly. If flow-induced surface deformations are neglected, the surface shape h(z) that is needed for the coordinate transformation can be determined a priori (Stojanovic et al., 2022). Otherwise, MaranStable computes h(z) simultaneously with the flow fields in the liquid and the gas, updating the coordinate transformation (1) after every iteration step.

Transforming the governing equations onto the computational domain  $(\xi,\eta)$  requires a transformation of the derivatives

$$\frac{\partial}{\partial r} = \frac{\partial \xi}{\partial r} \frac{\partial}{\partial \xi} := \xi_r \frac{\partial}{\partial \xi},\tag{2a}$$

$$\frac{\partial}{\partial z} = \frac{\partial \xi}{\partial z} \frac{\partial}{\partial \xi} + \frac{\partial \eta}{\partial z} \frac{\partial}{\partial \eta} := \xi_z \frac{\partial}{\partial \xi} + \eta_z \frac{\partial}{\partial \eta}, \tag{2b}$$

where the metric components

$$\xi_r \cong \frac{\Delta \xi}{\Delta r}, \qquad \xi_z \cong \frac{\Delta \xi}{\Delta z}, \qquad \eta_z \cong \frac{\Delta \eta}{\Delta z}$$
 (3)

are approximated by means of finite differences. Note that the second-order derivatives from the momentum and energy equations do not appear in the discretized set of equations owing to the finite volume method that is implemented in MaranStable. Figure 2 shows the collocation of the field quantities  $\bar{T}$ ,  $\bar{p}$ ,  $\bar{u}$  and  $\bar{w}$  on the structured and staggered grid. For the sake of simplicity, only the liquid phase is shown, where the free

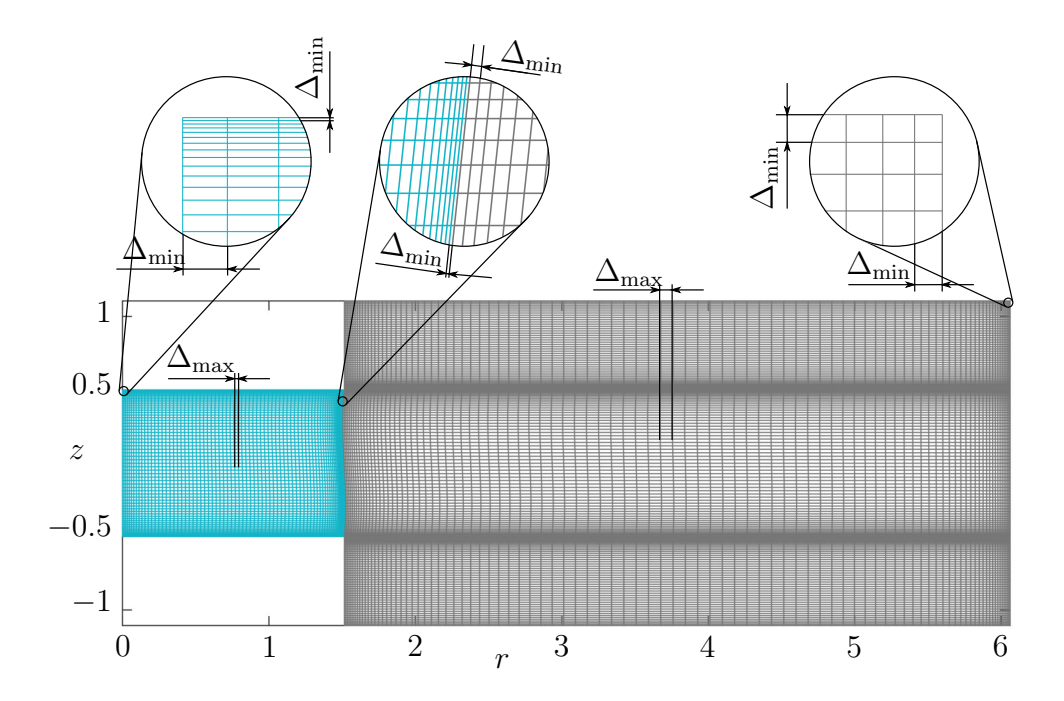


**Figure 3:** Example for the physical mesh inside the liquid (light-blue) and the gas (gray) with a total number of  $N_{\text{tot}} = 18\,852$  nodes. The coordinates have been made dimensionless using the height d of the liquid bridge. For better visualization, the total number of nodes was reduced by more than 80% compared to the default mesh.

surface is mapped to  $\xi \equiv 1$ . The overbar indicates the quantities are assigned to the computational mesh. The convective terms of the governing equations are discretized using a second-order central scheme, and the variables are linearly interpolated (Wesseling, 2009). Along the cell edges the variables and derivatives are treated as constants. The discretized nonlinear set of algebraic equations is solved by Newton–Raphson iteration.

Once the transformed governing equations are solved, MaranStable transforms the computed field quantities back into the physical variables, i.e. T, p, u, and w, for post-processing and the visualization. To that end, the infinitesimal variations of  $\xi$  and  $\eta$ 

$$d\xi = \frac{\partial \xi}{\partial r} dr + \frac{\partial \xi}{\partial z} dz \quad \text{and} \quad d\eta = \frac{\partial \eta}{\partial z} dz$$
 (4)

are expressed in terms of dr and dz. In matrix notation, the inverse transformation reads

$$\begin{pmatrix} dr \\ dz \end{pmatrix} = \underbrace{\frac{1}{\xi_r \eta_z} \begin{pmatrix} \eta_z & -\xi_z \\ 0 & \xi_r \end{pmatrix}}_{\mathbf{I}} \cdot \begin{pmatrix} d\xi \\ d\eta \end{pmatrix}, \tag{5}$$

where **J** is the Jacobian matrix. Applying (5) to the velocity components  $(u, w)^{\mathrm{T}} = \mathbf{J} \cdot (\bar{u}, \bar{w})^{\mathrm{T}}$  yields

$$u = \frac{1}{\xi_r} \bar{u} - \frac{\xi_z}{\xi_r \eta_z} \bar{w}, \quad \text{and} \quad w = \frac{1}{\eta_z} \bar{w}. \tag{6}$$

Since the scalar quantities do not suffer any transformation between the meshes,  $T = \bar{T}$  and  $p = \bar{p}$ .

To resolve the thermal and/or viscous boundary layers, MaranStable provides a grid refinement towards all boundaries. The user can choose between a hyperbolic-tangent profile or a geometric progression (Thompson et al., 1985). According to the stretching function selected for a particular space direction, the respective cell width grows in each direction from the user-defined width  $\Delta_{\min}$  of the wall cells (interface cells), until the user-defined width  $\Delta_{\max}$  inside the core region(s) are reached. Figure 3 shows a reduced version of the physical mesh for the geometry examined in Stojanovic et al. (2022).

## References

Stojanovic, M., Romanò, F. and Kuhlmann, H. C. (2022), 'Stability of thermocapillary flow in liquid bridges fully coupled to the gas phase', J. Fluid Mech. 949, A5 (51pp).

Thompson, J. F., Warsi, Z. U. and Mastin, C. W. (1985), *Numerical Grid Generation: Foundations and Applications*, Elsevier North-Holland, Amsterdam.

Wesseling, P. (2009), Principles of Computational Fluid Dynamics, Springer.